A technique to improve the design of near-zero energy buildings

Walter Mazuroski, Julien Berger, Benoit Delinchant, Frédéric Wurtz, Nathan Mendes

A Technique to Improve the Design of Near-Zero Energy Buildings

Walter Mazuroski[a,d*], Julien Berger [b], Benoit Delinchant[c], Frédéric Wurtz [c], Nathan Mendes [d]

[a] Univ. Grenoble Alpes, Univ. Savoie Mont Blanc, CNRS, LOCIE, 73000 Chambéry, France
[b] Laboratoire des Sciences de l'Ingénieur pour l'Environnement (LaSIE), UMR 7356 CNRS, La Rochelle Université, CNRS, 17000, La Rochelle, France
[c] Univ. Grenoble Alpes, CNRS, Grenoble INP, G2Elab, 38000 Grenoble, France
[d] Pontifícia Universidade Católica do Paraná, Rua Imaculada Conceição, 1155, CEP : 80215-901, Curitiba, Brazil
*corresponding author, e-mail address : walter.mazuroski@pucpr.br

Abstract

In the design context of Near-Zero Energy Buildings (nZEBs) and smart cities, robust and versatile optimization methods are needed to be coupled to simulation tools. In this way, the paper presents optimization algorithms coupled to a software with a capability to precisely simulate solar radiation availability by using a graphical `pixel counting` technique and by integrating with external models via Functional Mockup Interface (FMI). The optimization is based on mono- and multi-objective algorithms to solve a case study problem with two objectives to optimize: *i*) the cooling energy demand and *ii*) the payback period. Then, an economic viability model is presented, considering construction aspects such as insulation thickness, energy consumption and the number of installed solar panels. The algorithms are applied and compared for a building based on the BESTEST 910 case, considering tropical weather of Rio de Janeiro, Brazil. Both algorithms succeed, but with different characteristics related to computer run time and accuracy.

Keywords: Building optimization, Building energy efficiency, Economic viability in buildings, Mono- and multi-objective optimization, Photovoltaic energy generation.

1 Introduction

Energy and environment have been a major global concern in recent years. According to the last Brazilian Energy Balance [1], 51% of electricity consumption in the year 2018 was attributed to residential, commercial and public buildings. Also, energy used in buildings for heating, cooling and lighting comprises up to 23% of global energy-related CO_2 emissions, with one-third of those from direct fossil fuel consumption [2, 3]. Consequently, these data reveal the urgent need of building energy performance improvement dealing with sustainable design concepts. Therefore, it is imperative to use simulation tools for the design of optimal energy-efficient and environmentally friendly buildings.

The International Energy Agency (IEA), through Annex 52 titled "Towards Net Zero Energy Solar Buildings", is making an international effort to the standardization of the Net Zero Energy Building definition [4]. In the European Union, with the current directive [5, 6], the general trend is to design "nearly zero energy building", with very high energy performance and nearly zero or very low amount of energy required. This energy should be covered largely by energy from renewable sources, including energy from renewable sources produced on-site or nearby [5, 6]. Several studies have been carried out on the nZEB subject such as the impact of comfort parameters on the air conditioning energy demand for residential nZEBs [7] and the optimization of building envelope design for nZEBs in Mediterranean climate with multi-objective optimization algorithm [8]. Other investigations can be mentioned such as [9] or [10] on the enhancement of building energy efficiency through building information modeling.

The design of sustainable buildings is not a simple task as it must achieve high levels of performance at the lowest possible cost, with the possibility of a large space of solutions and many physical processes that lead to conflicting objectives. To deal with these difficulties it is worth to apply computational methods of design optimization [11]. A recent review on the use of genetic algorithms for building retrofitting optimization is proposed in [12]. Several recent illustrations of multi-objective optimization can be mentioned as [13] for energy policies at larger scales or [14] and [15] for building stocks retrofit. In [16] multi-optimization approach is used to choose among several energy efficiency measures. Last, [17] investigate the retrofitting of social houses by combining dynamic building energy simulations and multi-objective optimization.

There are several ways to solve optimization problems. The weighted sum is a classical approach to solve a multi-objective optimization problem, assigning weights to each normalized objective that is converted to a single-objective problem, which is solved using a mono-objective algorithm [18]. Another approach is the Pareto multi-objective optimization, where a range of solutions are sought that enclose the trade-off among the objectives. Regarding multi-objective algorithms, the most commonly used is the `NSGA-II` (Non-dominated Sorting Genetic Algorithm-II), a robust multi-objective optimization genetic algorithm [19]. A reference-point based variation named `NSGA-III` is suggested in [20].

A comprehensive review of all significant research applying computational optimization to sustainable building design problems, covering 74 works with a focus on different fields of sustainable building design is presented in [11]. Furthermore, a methodology and an environment allowing the interoperability of numerical tools for the holistic optimization of buildings is presented in [21], with an optimization case study based in a real building.

This interest in tools that enable building optimization is the main motivations of this work, intending to bring an optimization tool integrated to a BES tool, as well as assisting the design of more efficient building projects.

In this paper, two optimization algorithms are integrated into a Building Energy Simulation (BES) tool to optimize energy and construction economic viability. The optimization considers sophisticated graphical resources such as `pixel counting` to accurately and rapidly assess the sunlit radiation on PV panels and building facades. In order to promote more in-depth analyses of different optimization approaches, a comparison between mono- and multi-objective algorithms to optimize a multi-criteria problem is performed.

The article is organized as follows. The building energy simulation program `Domus` and the building economic analysis model are described in Section 2. Then, the mono- and multi-objective optimization models are presented in Section 3. A presentation of the case study and its optimization results is carried out in Section 4. To conclude, final remarks are addressed in Section 5.

2 Methodology

2.1 The building energy simulation program Domus

The whole-building hygrothermal and energy simulation program `Domus` is used as the building energy simulation tool, being able to compute the room air temperature using the lumped multizone model [22, 23]. The energy balance of the zones is performed considering heat exchanged with walls, windows, occupants, lighting, equipment and HVAC systems. `Domus` has been used in a variety of studies as in [24] that presented integrated calculation of the hygrothermal behavior of indoor climate, building porous envelope and central HVAC system. The work presented in [25] validates several cross and single-sided natural ventilation models implemented in `Domus`. Another example is the study presented by [26] to analyze the modeling level needed to successfully evaluate the heat transfer through window glazing materials in whole-building simulation.

Photovoltaic panels (PV) are numerically coupled in `Domus` in the work presented by [27]. Using `Domus`, the user can select any building zone external surface to add photovoltaic panels to the building envelope as a building-integrated photovoltaic (BIPV) strategy. The BIPV effect on the heat transfer through the building envelope is also considered on energy performance assessment, including information on the number of panels, panel size, thermophysical properties and model. The `pixel counting` technique provides accurate calculation of direct solar radiation on the solar panels (Figure 1), regardless of the geometry and the presence of shading elements.

Among the possibilities of using `pixel counting` in building simulation, there is the one presented in [28] for designing shading devices considering energy efficiency, daylight, and fading protection. An extensive validation presented in [29] and [30] shows how the use of this technique could bring an accurate and fast assessment of sunlit surface fraction even for complex geometries.

`Domus` has been written in C++ with an OpenGL based graphical interface and can consider moisture sorption effects. Additional information is available at `http://domus.pucpr.br/` (in portuguese).

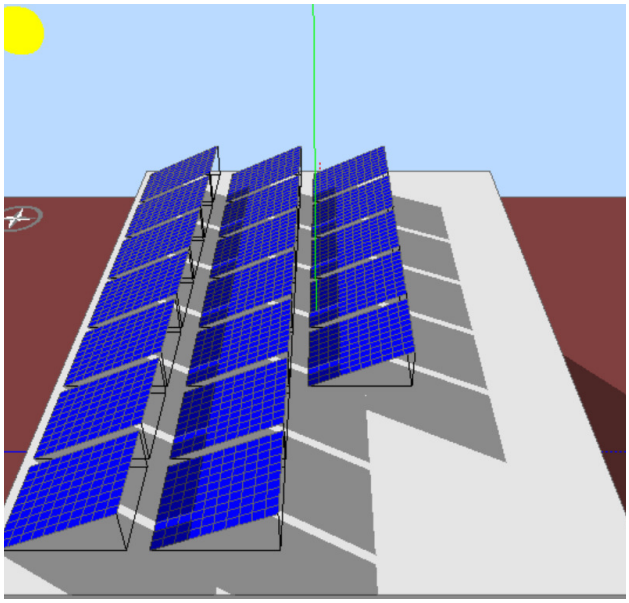

Figure 1. *`Domus` solar panels with sunlit calculations based on pixel counting.*

2.2 Economic analysis

To assess the economic viability of the project, a simple economic analysis, based on the payback-time, is proposed according to [31, 32]. The objective is to calculate the time required to pay for the investment in insulation and solar panels using the commercialization of the energy generated by the photovoltaic system. The energy consumption with ventilation and solar power equipment maintenance is also considered. Although HVAC equipment's cost can also be reduced according to demand, this specific cost is not considered in this model.

The economic viability of the project τ [years] comes from the solution of the following equation:

$$C_{inv} + (C_{eg} + C_{ec} + C_m)\,\tau = 0\,, \tag{1}$$

where C_{inv} [\$], C_{eg} [\$], C_{ec} [\$] and C_m [\$] are the investment cost, the energy generation cost, the energy consumption cost and the maintenance cost, respectively. Rearranging the

equation, the economic viability of the project can be expressed as:

$$\tau \;=\; \frac{-\,C_{inv}}{C_{eg} \;+\; C_{ec} \;+\; C_m}\,. \tag{2}$$

In addition, the following convention is adopted: negative costs that spend financial resources (C_{inv}, C_{ec} and C_m); positive costs that generate financial resources (C_{eg}). The investment cost C_{inv} $[\,\$\,]$ is evaluated according to:

$$C_{inv} \;=\; -\,A\,c_{p,0} \;-\; p_i\,A_i\,l_i\,, \tag{3}$$

with A $[\,\mathsf{m}^2\,]$ as the area of the solar panels, $c_{p,0}$ $[\,\$\,.\,\mathsf{m}^{-2}\,]$ the installation cost of solar panels, p_i $[\,\$\,.\,\mathsf{m}^{-3}\,]$ the insulation price, A_i $[\,\mathsf{m}^2\,]$ the surface of the insulation and l_i $[\,\mathsf{m}\,]$ the length of insulation. The energy generation cost C_{eg} is given by:

$$C_{eg} \;=\; E_p\,A\,p_s\,, \tag{4}$$

where E_p $[\,\mathsf{kWh}\,.\,\mathsf{m}^{-2}\,]$ is the electricity produced by the panels computed by the `Domus` simulation program according to the model [27]. The quantity p_s $[\,\$\,.\,\mathsf{kWh}^{-1}\,]$ is the selling price of electricity. The energy consumption cost C_{ec} is:

$$C_{ec} \;=\; -\,(\,E_{ac} \;+\; E_v\,)\,p_e\,, \tag{5}$$

with E_{ac} $[\,\mathsf{kWh}\,]$ being the electric energy consumption of the air conditioning system, directly computed by `Domus` and p_e $[\,\$\,.\,\mathsf{kWh}^{-1}\,]$ the electric energy price. The ventilation system energy consumption E_v $[\,\mathsf{kWh}\,]$ is given by:

$$E_v \;=\; S_{fp}\,t\,q\,, \tag{6}$$

where S_{fp} $[\,\mathsf{kW}\,.\,\mathsf{m}^{-3}\,.\,\mathsf{s}\,]$ is the specific fan power [33], t $[\,\mathsf{h}\,]$ is the time of use and q $[\,\mathsf{m}^3\,.\,\mathsf{s}^{-1}\,]$ the ventilation airflow rate. Last, C_m $[\,\$\,]$ is the photovoltaic system maintenance cost is based in the interest compound formulation [16, 34–36] and given by:

$$C_m \;=\; -\,(\;1.0+\omega\;)^A\,c_{p,0}\,, \tag{7}$$

where the coefficient ω $[\,-\,]$ represents a ratio cost on an annual base. The maintenance cost is defined as exponential since its probability distribution describes failure may appear at any time [16, 35–37]. At last, Equation (2) can be presented in full as:

$$\tau \;=\; \frac{A\,c_{p,0} \;+\; p_i\,A_i\,l_i}{E_p\,A\,p_s \;-\; (\,E_{ac} \;+\; E_v\,)\,p_e \;-\; (\;1.0+\omega\;)^A\,c_{p,0}}\,. \tag{8}$$

Before that, τ is the number of years that verifies equation (1) and consequently fulfills the objective of paying the investment cost by means of the energy generated by the photovoltaic system.

3 Optimization

The main objective of this work is the coupling of an optimization model with a BES modeling an accurate assessment of direct solar radiation availability. This section describes the two adopted approaches that are used to solve the multi-criteria problem by employing mono- and multi-objective strategies. The coupling interface to perform the communication between the `Domus` tool and optimization models is the FMI [38]. The latter is a free standard defining a container and an interface to carry exchanges of information between dynamic model. It can be used for co-simulation, where each model has its own numerical solver, or for model exchange, where the connection is done to a numerical solver. The second option is employed here. Each model is exported into a Functional Mock-up Unit (FMU) so that the exchange between models can be operated.

3.1 Parameter space for the optimization problem

The algorithm starts with the initialization step, where `Domus` utilizes the user-defined input configurations to define the parameters space Ω:

$$\Omega \;=\; \bigcup_{i\,=\,1}^{N_p} \Omega_i \,, \tag{9}$$

where N_p the total number of parameters and Ω_i is the space for each parameter considering the user-defined minimum and maximum values and given by:

$$\Omega_i \;=\; \{\, p_i \in \mathbb{R} \mid p_i^{\min} \leqslant p_i \leqslant p_i^{\max} \,\} \,. \tag{10}$$

The group of parameters to be optimized $\boldsymbol{p}$ is composed of elements of the parameter space Ω and given by:

$$\boldsymbol{p} \;=\; (\, p_i \,) \quad \text{for} \quad i \;=\; \{1..N_p\} \,. \tag{11}$$

The set Ω is transmitted to the optimization FMU through the FMI interface.

The objectives space Γ is the space generated for evaluation of the objective functions for all values in Ω and given by:

$$\Gamma \;=\; \bigcup_{i\,=\,1}^{N_o} J_i(\Omega) \,, \tag{12}$$

where N_o is the number of objectives and J_i is the objective function for each i-objective.

3.2 Mono-objective optimization with a surrogate-based algorithm

The purpose of mono-objective optimization is to find the most efficient building configuration in terms of energy consumption and economic viability. Since only one objective can be optimized in this approach, two terms are combined in one balanced objective function J:

$$J(\boldsymbol{p}) \;=\; w_1 \cdot J_1(\boldsymbol{p}) + w_2 \cdot J_2(\boldsymbol{p}) \,, \tag{13}$$

with J_1 being the relative value of cooling energy demand:

$$J_1(\boldsymbol{p}) \;=\; \frac{E_{ac}(\boldsymbol{p}) - E_{ac}^{\min}}{E_{ac}^{\max} \;-\; E_{ac}^{\min}} \,,$$

and J_2 the relative value of the economic model result:

$$J_2(\boldsymbol{p}) \;=\; \frac{\tau(\boldsymbol{p}) - \tau^{\min}}{\tau^{\max} \;-\; \tau^{\min}} \,,$$

where min and max are the minimal and maximal values expected for each objective and w_1 and w_2 are weights to balance the objectives. The optimization search for the set of parameters:

$$\boldsymbol{p}^{\circ} \;=\; \min_{p} J(\boldsymbol{p}). \tag{14}$$

The optimization technique chosen is the Bayesian one that attempts to find the global optimum in a minimum number of steps. The model used in this technique for approximating the objective function is called a surrogate model. The Bayesian optimization considers an acquisition function that directs sampling to areas where an improvement over the current best observation is likely [39–41]. The surrogate model-based optimization algorithms will be referred to in this work as `Kriging model`.

The mono-objective optimization starts after the space parameters definition, with the generation of the initial set of data points, denoted Ω_s, generated using the Latin Hypercube Sampling (LHS) technique:

$$\Omega_s \;=\; \{\, \boldsymbol{p}_s \}_{s=1}^{N_s}\,, \tag{15}$$

where N_s is the number of initial data points defined by the user. The set of initial points Ω_s is transmitted back to `Domus` to compute Γ_s, the set of objective function for each element of Ω_s:

$$\Gamma_s \;=\; \{\, J(\boldsymbol{p}_s) \}_{s=1}^{N_s}\,, \tag{16}$$

The results are provided to the `Kriging model`. This sampling enables a first rough approximation of the objective function by the surrogate model. The second part of the process starts with `Domus` receiving a new group of parameters $\boldsymbol{p}^\star$ provided by the `Kriging model` to improve the approximation of the objective function. `Domus` apply the parameters to the project and execute a new simulation returning the $J(\boldsymbol{p}^\star)$ as an objective function result to the `Kriging model`.

The optimization process ends when reaching the total number of simulations ($N_{tot} \;=\; N_s + N_k$) - where N_k is the user-defined maximum number of kriging iterations - or satisfied one of the following criteria:

$$\gamma_1 \;\leqslant\; \eta_1 \qquad or \qquad \gamma_2 \;\leqslant\; \eta_2\,, \tag{17}$$

where η_1 and η_2 are user-defined values and λ, the number of previous iterations considered to evaluate the convergence. The criteria γ_1 and γ_2 assess the relative magnitude changes in the objective function and in the candidate parameters that result in the minor objective value, respectively:

$$\gamma_1 \;=\; \sum_{i \,=\, k-\lambda}^{k} \frac{\parallel J(\boldsymbol{p}_{i+1}^{\circ}) \;-\; J(\boldsymbol{p}_i^{\circ}) \parallel_2}{\parallel J(\boldsymbol{p}_i^{\circ}) \parallel_2}\,, \qquad \gamma_2 \;=\; \sum_{i \,=\, k-\lambda}^{k} \frac{\parallel \boldsymbol{p}_{i+1}^{\circ} \;-\; \boldsymbol{p}_i^{\circ} \parallel_2}{\parallel \boldsymbol{p}_i^{\circ} \parallel_2}\,. \tag{18}$$

The adopted methodology used to implement a mono-objective optimization tool in the `Domus` software is illustrated in Figure 2a and the FMU developed was implemented integrated with `Python` scripts based on Gaussian Process Regression (GPR) using the `Scikit-optimize` library available into the `scikit-learn` library [42], using the quasi-Newton method as a minimization function. A procedure chart of the whole process is illustrated in Figure 2b. Furthermore, Table 1 lists the computer programs involved for the mono-objective optimization procedure. Note that `Python` is used at several levels: for generating the initial data-set (Latin Hypercube Sampling), for the optimization using the `Kriging model` and for the stopping criteria.

3.3 Multi-objective optimization with `NSGA-III`

The purpose of the multi-objective optimization is to find the *Pareto optimal parameters set* and its corresponding objective function values (*Pareto front*). Since it is not computationally feasible to investigate all the parameters set to find the *true Pareto front*, it is imperative to use an approach to identify a set of solutions (*the best-known Pareto set*) that represent the Pareto optimal set as much as possible [18]. The approach used is the Reference-point Based Non-dominated Sorting Approach (`NSGA-III`). Based on the `NSGA-II` algorithm, the Reference-point Based approach emphasizes population members who are non-dominated yet close to a set of supplied reference points [43].

The objectives that compose the objective space are the cooling energy demand J_1:

$$J_1(\boldsymbol{p}) \;=\; E_{ac}(\boldsymbol{p})\,,$$

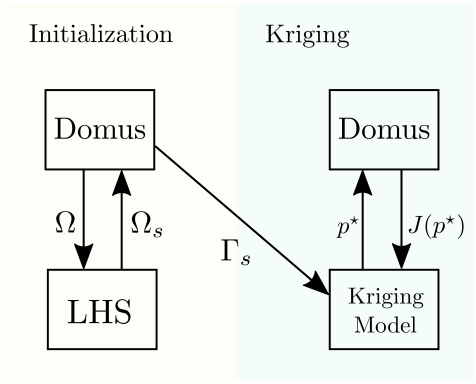

(a)

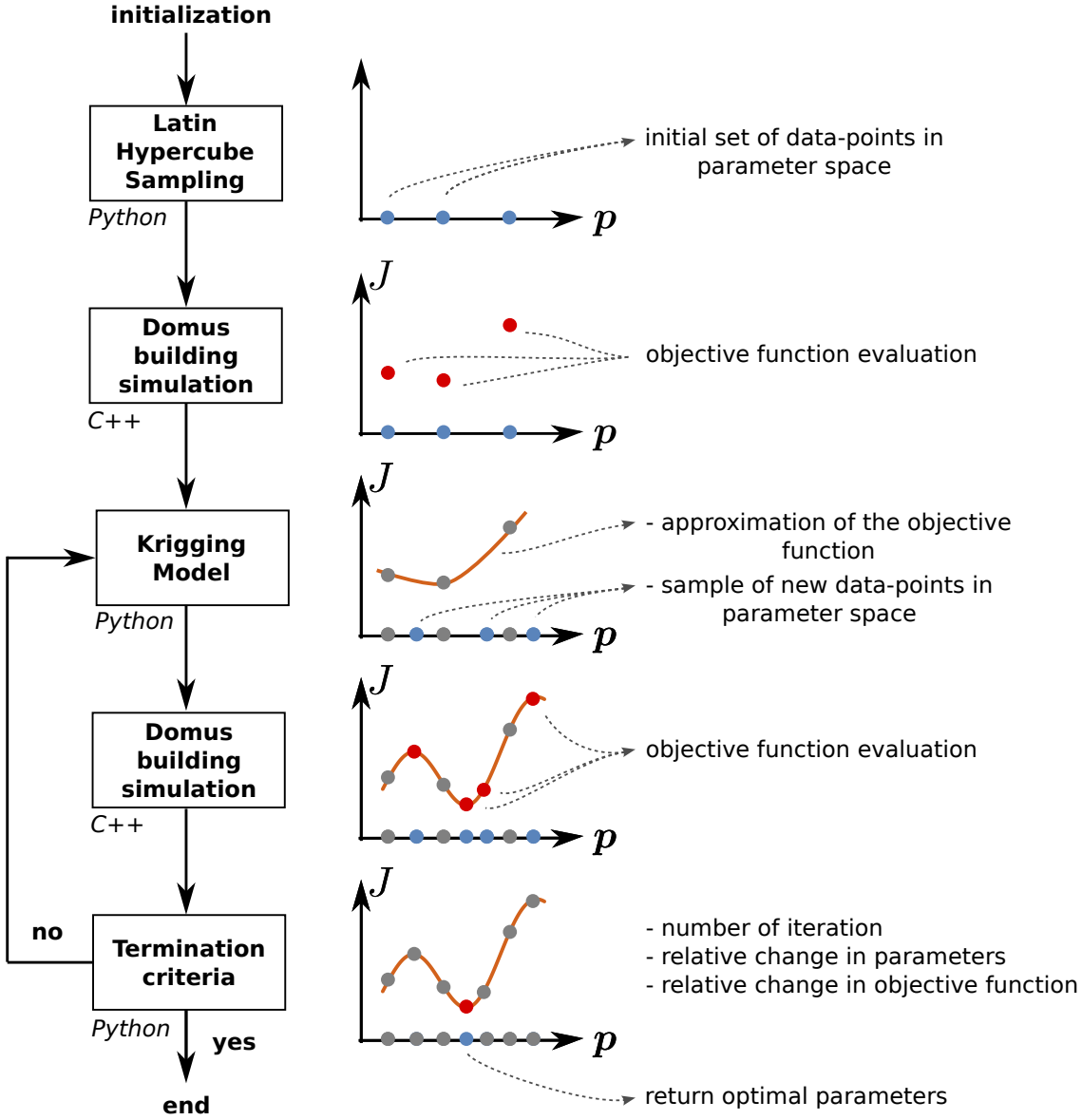

(b)

Figure 2. *Adopted methodology* (a) *and procedure chart* b *for the mono-objective optimization.*

and economic viability J_2:

$$J_2(\boldsymbol{p}) \;=\; \tau(\boldsymbol{p})\,.$$

As a multi-objective optimization, it is possible to optimize both objectives at the same time. Figure 3 presents the methodology adopted for the multi-objective optimization using `Domus` and the FMI interface, with an FMU elaborated employing `NSGA-III` library available in DEAP [44].

The multi-objective model presents two new parameters in addition to what is presented for the mono-objective. The first one is the population's size N_u, which can ensure diversity in the obtained solutions and must be defined according to the number of objectives [43]. The second configuration is the number of generations N_g. For each generation, `Domus` will perform N_u simulations for each generation required. Both are user-defined configurations. Other more specific configurations for the `NSGA-III` are kept in the default value.

After `Domus` supplying the space parameters definition to the `NSGA-III` model, an initial generation set, denoted Ω_g, is created:

$$\Omega_g \;=\; \{\,\boldsymbol{p}_u\}_{u=1}^{N_u}\,, \tag{19}$$

This first generation set Ω_g is transmitted back to `Domus` to compute Γ_g, the set with objective function values for each element of Ω_g:

$$\Gamma_g \;=\; \{\,E_{ac}(\boldsymbol{p}_u),\,\tau(\boldsymbol{p}_u)\,\}_{u=1}^{N_u}\,, \tag{20}$$

After concluded the initialization step, the optimization process starts with `Domus` receiving a new generation set Ω_g provided by the `NSGA-III` model to improve the *best-known Pareto Front*. `Domus` simulates each element of this set and returns the new Γ_g to the optimization model.

The optimization process ends when reaching the user-defined total number of generations N_g, or through direct intervention, in case the user believes the optimization achieved a satisfactory result. The procedure chart for the multi-objective optimization is very similar to the one illustrated in Figure 2b. Instead, the LHS and `Kriging model` are performed by the NSGA entirely. Table 1 lists the computer programs involved for the multi-objective optimization procedure. Here, the `Python NSGA-III` algorithm from the DEAP library is employed.

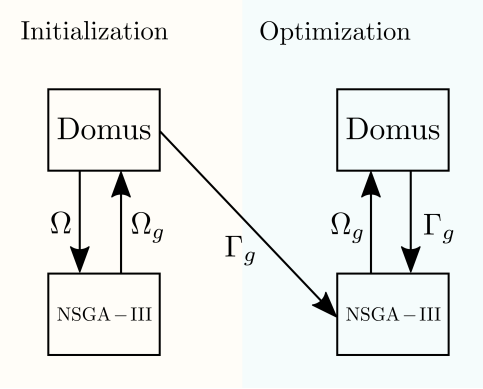

Figure 3. *Adopted methodology for the multi-objective optimization.*

4 Results and discussion

4.1 Mono-objective model implementation verification

In order to verify the implementation of the optimization model in the FMI interface, a standalone test was carried out based on the Ackley function (Figure 4). The objective function

Table 1. *List of computer programs used.*

	Computer program	*Role*
Mono-obj.	`Python`	Latin Hypercube Sampling for the generation of the initial set of data-points
	`Domus`	Building simulation program that evaluates the mono-objective function
	`Python`	`Kriging model` to improve the approximation of the objective function
	`Python`	`Scikit-optimize` library for the stopping criteria
Multi -obj.	`Domus`	Building simulation program that evaluates the multi-objective function
	`Python`	DEAP–`NSGA-III` to improve the pareto front and carry the multi-objective optimization

of this test is:

$$J(p_1, p_2) = -20 \exp\left(-0.2\sqrt{\frac{1}{2}\sum_{i=1}^{2} p_i^2}\right) - \exp\left(\frac{1}{2}\sum_{i=1}^{2}\cos\left(2\pi p_i\right)\right) + 20 + \mathrm{e}\,.$$

This two-dimensional ($N = 2$) test function is characterized by a nearly flat outer region, and a large hole at the center. Presenting many local minima this function can be a challenge for optimization algorithms [45, 46]. The global minimum is $J(p_1^0, p_2^0) = 0$ with $p_1^0 = p_2^0 = 0$ and range used for the model verification is $(p_1, p_2) \in [-5; 5]^2$.

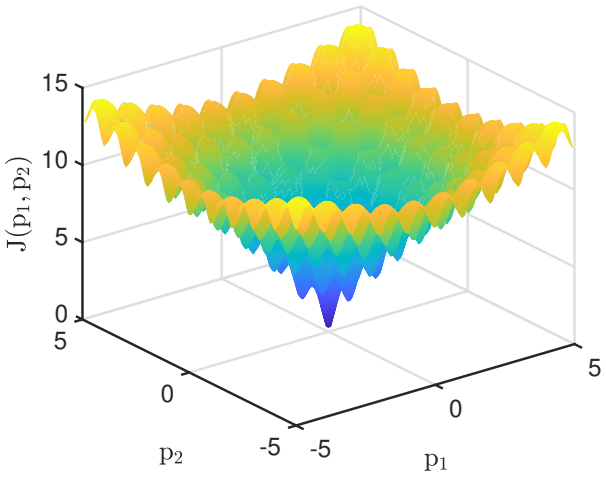

Figure 4. *Ackley Function.*

A python script was developed to perform the validation of the implementation of optimization. The validation used the *scikit-learn* library for optimization and the LHS method to generate the initial set of samples, a total of 300 iterations with the first 5 being the initial set. The results bring the convergence of the minimum objective function (Figure 5a), where it is possible to observe that after 196 iterations the optimization algorithm calculated a value around 0.04 as the minimum objective value and no more variation until the end. The respective parameters are presented in Figure 5b.

The results show that despite the function having many local minima, the optimization algorithm successfully managed to locate the region of the global minimum in less than 100 iterations, in the following iterations it was possible to get even closer to the global minima, showing a satisfactory performance even considering that no more in-depth study of model configuration was performed.

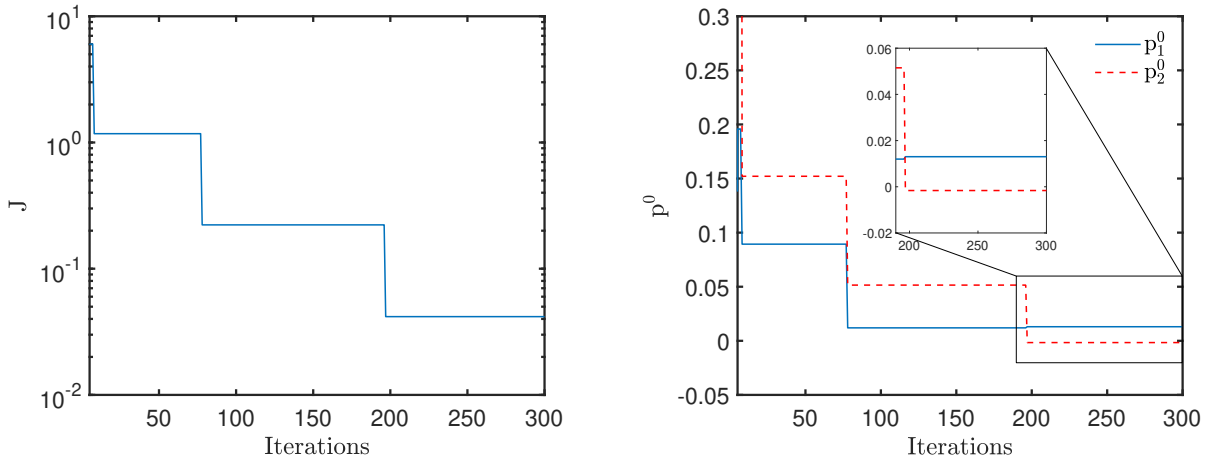

Figure 5. *Convergence plot of the minimum objective function J (a) and the respective parameters to obtain the minimum value of J (b).*

4.2 Multi-objective model implementation verification

The validation of the utilization of `NSGA-III` in `Domus` through the FMI interface was done using the test case using DTLZ2 multi-objective problem, presented in the documentation of the library `DEAP`. The results presented a good agreement with the reference result of the DTLZ2.

4.3 Presentation of the case study

The basic test building (Figure 6) is located in Rio de Janeiro, Brazil, where cooling loads are considerably high. The geometry consists of a rectangular shaped single zone ($8\,m$ wide x $6\,m$ long x $2.7\,m$ high) with no interior partitions and $5.88\,m^2$ (2 windows of $2.1\,m$ wide x $1.4\,m$ high) North-oriented windows located at $0.6\,m$ from the ground. Based on the BESTEST 910 high mass building model, this building is a heavyweight type construction with characteristics described in Tables 7 and 8 of Appendix 5. There is also a $1-m$ horizontal overhang across the entire width of the wall with windows at the roof level. Adapting to Brazilian standards, the size of windows has been reduced from $12\,m^2$ to $5.88\,m^2$. The window glazing properties (Table 9 of Appendix 5) correspond to the NFRC-102 ones (Window 5, 1995). The original orientation of the base case has been changed from South to North, as the analysis is carried out for the southern hemisphere. The floor was defined as adiabatic as a simplification of the model. A ventilation air change rate is assumed to be equal to 0.5 ach (air changes per hour). Internal heat gain of $200\,W$ (60% radiative, 40% convective, 100% sensible) is considered as a constant during the whole period. The mechanical system is 100% convective air system, 100% efficient with no duct losses and no capacity limitation, no latent heat extraction, non-proportional-type dual setpoint thermostat with deadband (heating $< 20^oC$, cooling $> 27^oC$). For further details refer to Section 5.2.1 of ANSI/ASHRAE Standard 140-2007.

The choice of a case study based on the BESTEST 910 model was done because it is a well-known high mass building. Another point that influenced the choice was the presence of insulation in the composition of the BESTEST 910 vertical walls, with the objective of optimizing the thickness of the insulation material. In addition to the BESTEST 910 model previously described, solar panels will be included on the roof for the cooling demand system of the building.

Regarding the configuration of the economic model for the present case study, the parameters defined are shown in Table 2. These values are based on local market costs at the time of the investigation [47–49].

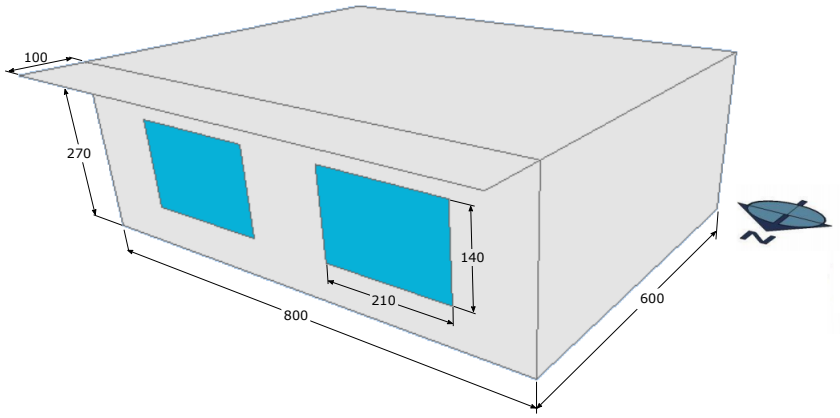

Figure 6. *Base building (modified Case 910).*

Table 2. *Economic model configuration parameters (taken in October 2020).*

$c_{p,0}$ $[\$.\mathrm{m}^{-2}]$	p_i $[\$.\mathrm{m}^{-3}]$	p_s $[\$.\mathrm{kWh}^{-1}]$	p_e $[\$.\mathrm{kWh}^{-1}]$	S_{fp} $[\mathrm{kW}.\mathrm{m}^{-3}.\mathrm{s}]$	ω
130	30	0.064	0.13	1	0.075

4.4 The need of optimizing the original case

The optimization need was evaluated using a period from the 10^{th} to the 13^{th} of January (summer in Brazil). Figures 7a and 7b enable to verify the influence of each element on the thermal loads of the building. The first one presents the gains ϕ from the walls for the case study without optimization and the second one other relevant gains in the zone. It is possible to conclude that the window glass does not generate considerable heat gain inside the zone for the evaluation period, with a maximum value close to 150 W. The vertical walls indeed represent a significant influence, with values close to 1200 W.

Windows may have a greater impact on the building envelope cooling loads depending on parameters such as window-to-wall ratio, azimuth, frame quality and thermophysical properties of both opaque and translucid components. In the present case, we have modified the BESTEST case, by reducing the size of the windows and by providing a large overhang, which decreases significantly the importance of the window thermal gains when compared to those associated to the heat transmitted through the opaque parts.

Figures 7a and 7b show the influence of different parts on thermal loads. The first one presents envelope related thermal gains while the second one compares the thermal gains through windows with the gain associated to the ventilation. The solar radiation thermal gain is related to the solar radiation passing through the windows, which is low due to very high position of the sun combined with the presence of the overhang. The window conduction loads are not high either when compared to the walls due to the difference between the areas and the thermal properties of the materials used in the simulation. As mentioned in the paragraph above, the glazing part does not play the major role for the modified BESTEST case, during the evaluation period (10^{th} to the 13^{th} of January) for the optimization analysis, with a maximum value close to 150 W. The vertical walls indeed represent a significant influence, with values close to 1200 W. Similar analysis can be carried out using Figure 11 for the whole year. Note that these results stand for the case study without optimization.

The windows model `Domus` uses is based on an unsteady finite-difference based model presented in [26, 50–52]. To calculate direct solar radiation gains on external and internal surfaces, `Domus` uses a pixel counting technique since it provides accuracy and rapidness for any geometry as demonstrated in [28–30, 53] and mentioned in Section 2.1.

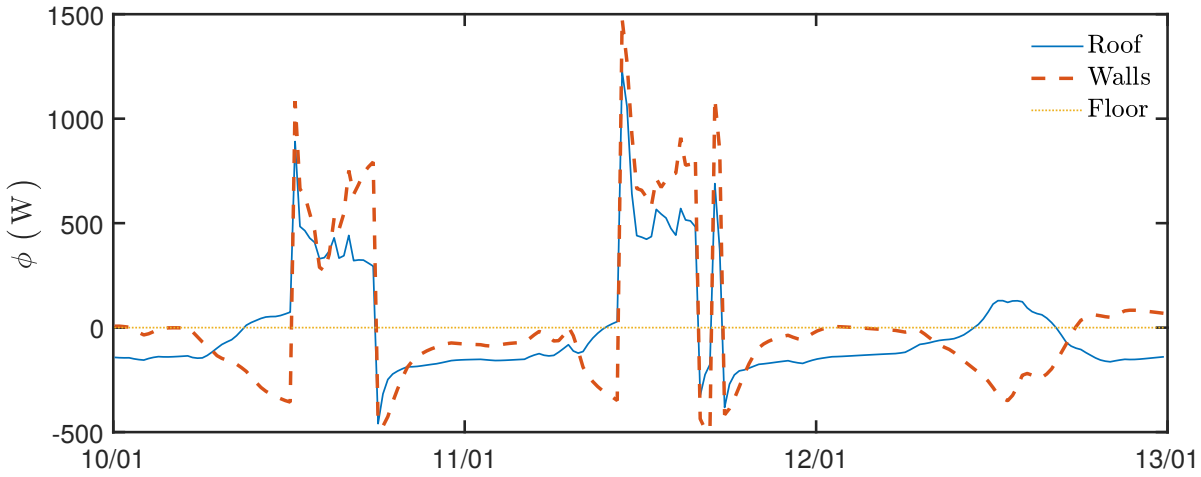

(a)

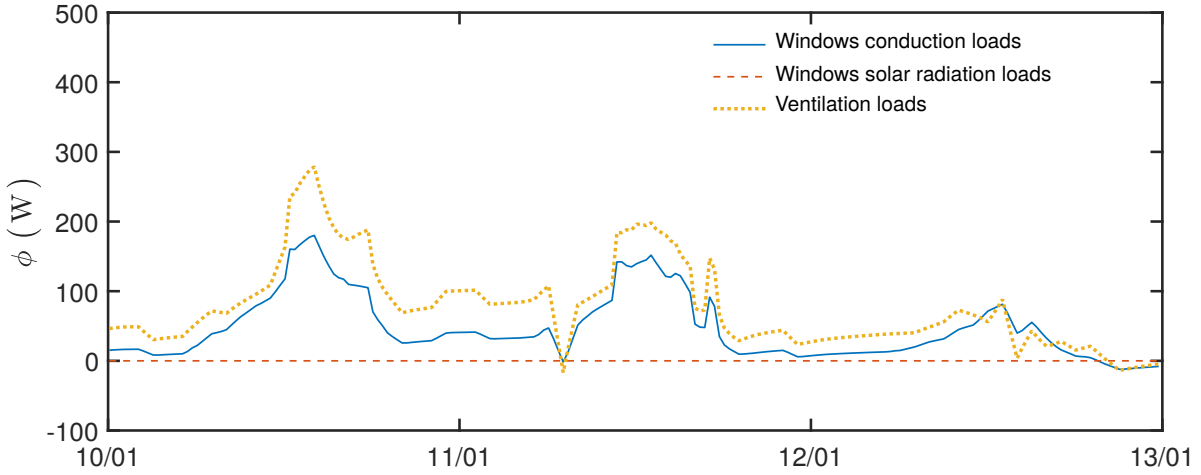

(b)

Figure 7. *Wall thermal gains (a) and other significant thermal gains (b) for the original project.*

The vertical walls generate more heat gain in all scenarios, including the one with minimum insulation thickness. Moreover, in Figures 8a and Figures 8b, it is possible to observe the differences comparing low and high thicknesses of insulation. As in the Bestest case, the floor is considered adiabatic.

The internal temperature and external climate temperature have a strong influence on the thermal gains as shown in Figure 9. Figure 10 presents the effect of the activation of the cooling system on the thermal gains.

The effect of insulation on the activation periods of the cooling system (Figure 10) is noticeable. Since conduction loads in the present case have a high impact on energy demand and consumption, the insulation of all vertical walls and the ceiling are defined as the first parameter to be optimized (denoted l_i). The second parameter will be ventilation airflow (denoted q_v). Since air quality or mould growth is not presently monitored, the expected effect of ventilation in a tropical climate on the air conditioning system should be optimized to its lowest value. Finally, the third parameter is the number of solar panels (denoted n_p), for energy production, also considering the cost of the equipment by means of the economic model. As remarked in Figure 12, there is a significant sink of solar radiation that can be directly used for solar panels

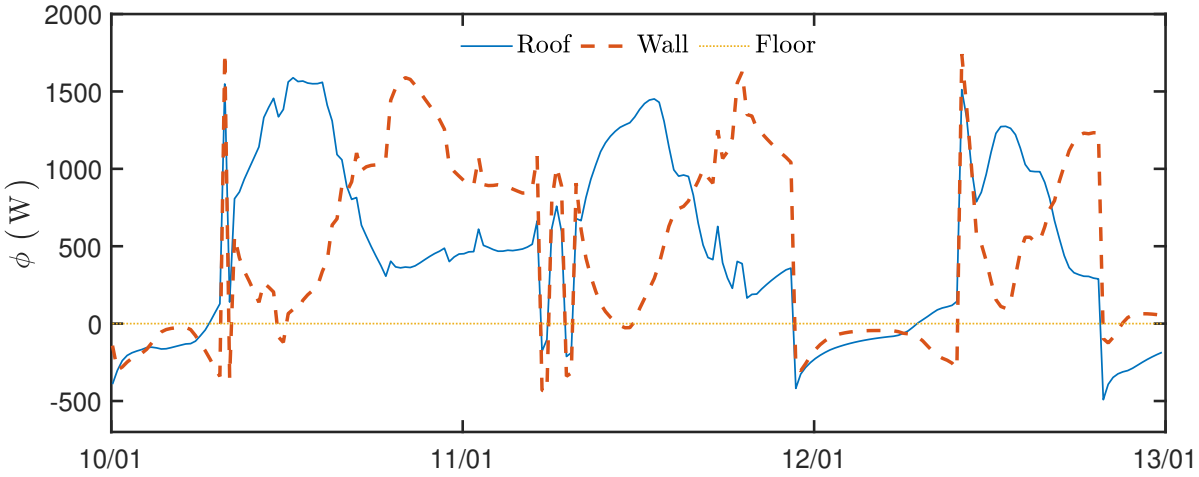

(a)

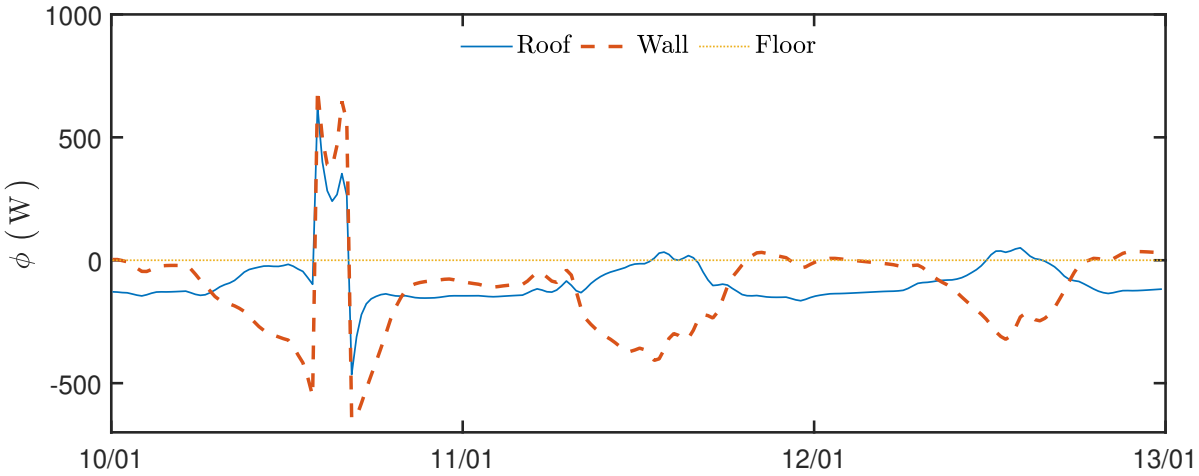

(b)

Figure 8. *Wall thermal gains for minimum value of insulation (5 mm) (a) and for maximum value of insulation (300 mm) (b).*

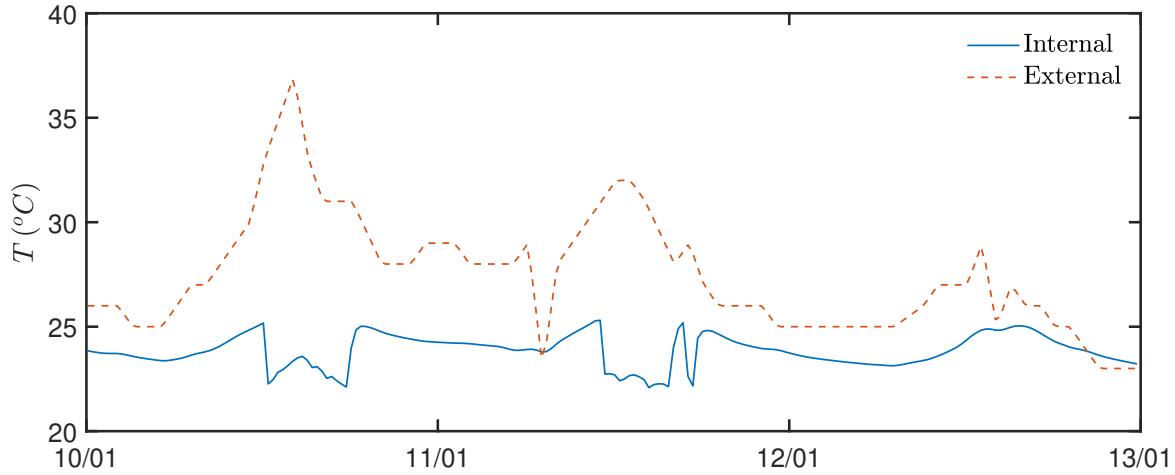

Figure 9. *Internal and external temperatures.*

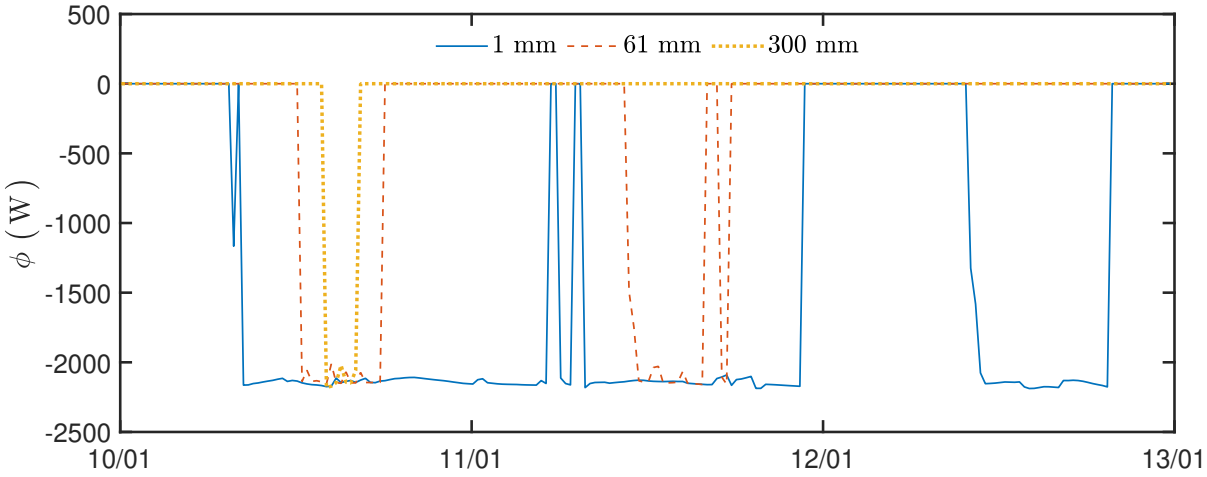

Figure 10. *Cooling demand for different values of insulation.*

to reduce the use of fossil energy. The use of solar panels is enhanced as the peak of cooling demand occurs during the day (Figure 10).

Considering the described parameters, the set of parameters $\boldsymbol{p}$ for the case study can be defined as:

$$\boldsymbol{p} = (l_i, q_v, n_p)\,. \tag{21}$$

Consequently, the set of optimized parameters can be described as:

$$\boldsymbol{p}^{\circ} = (l_i^{\circ}, q_v^{\circ}, n_p^{\circ})\,. \tag{22}$$

The reduction of solar conversion efficiency is noticeable for the hottest periods (Figure 12). Even so, during most of the year, the energy generated by the PV system is sufficient to supply the need for cooling demand. The temperature effect on the PV efficiency is part of the implementation of the model in `Domus`, as presented in [27].

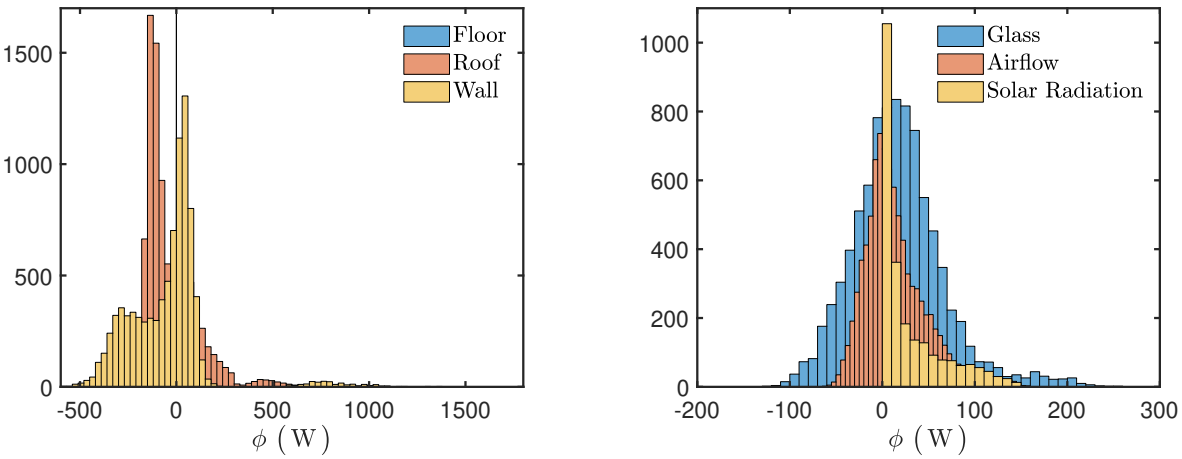

Figure 11. *Histogram of thermal gains during 1 year for zone walls thermal gains(a) and other significant thermal gains(b).*

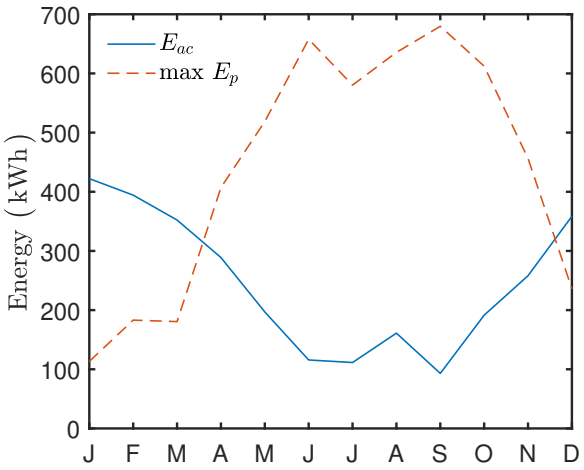

Figure 12. *Energy demand E_{ac} and solar panel energy production E_p, considering the maximum number of solar panels that can be installed.*

4.5 Mono-objective optimization

4.5.1 Results

The mono-objective optimization considers $N_s = 25$ initial LHS samples and more $N_k = 50$ kriging iterations with stopping criteria and configurations as described in Table 3. From a $N_{tot} = 75$, the optimization finished after reaching convergence in γ_1 with 37 kriging iterations and a total of 62 simulation runs. Figure 13 shows the cooling demand comparing the original design based on the BESTEST 910, the optimized design and also comparing with a randomly configured design (Table 4), while Figures 14a and 14b show the individual calculated costs and the economic viability of the project in terms of $\tau[\,\text{years}\,]$, respectively.

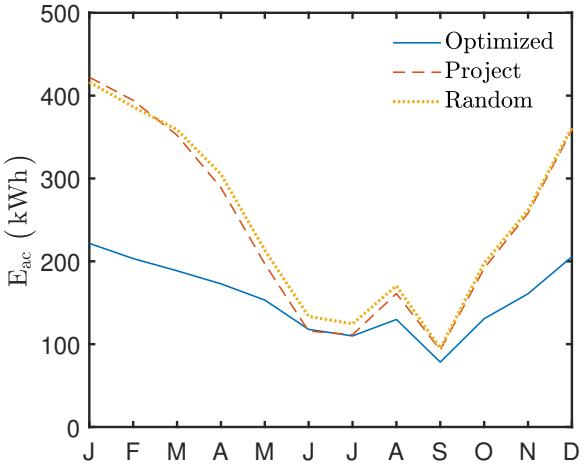

Figure 13. *Annual cooling demand for optimized, original and a random project.*

The optimized design correctly fulfills both the objectives of reducing both cooling demand throughout the year and the payback time with the investments in solar panels and insulation .

Table 3. *Mono-objective optimization configuration.*

w_1	w_2	$E_{ac}^{\min}$	$E_{ac}^{\max}$	$\tau^{\min}$	$\tau^{\max}$	η_1	η_2	λ
0.5	0.5	0	5000	0	10	0.001	0.001	10

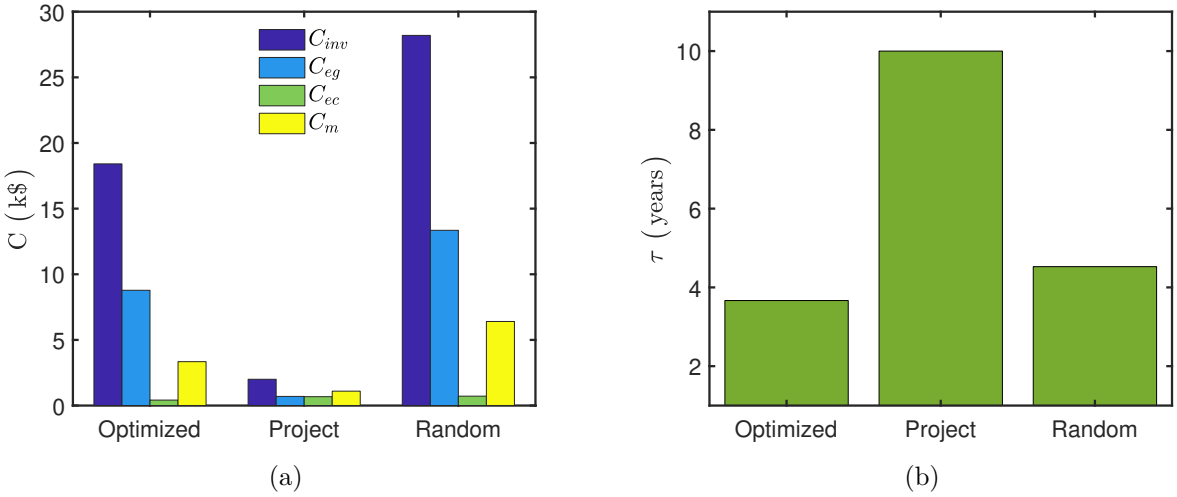

Figure 14. *Costs (a) and τ value (b) for optimized, original and a random project.*

Table 4. *Parameters of the projects*

Project	l_i [mm]	q_v [m3/h]	n_p [−]	E_{ac} [kWh]	τ [years]
Original	61	64.8	1	2943.79	10
Optimized	160	5.0	17	1898.13	3.66
Random	210	107.57	20	3024.66	4.52

For comparison purposes, Figures 15a and 15b show the thermal gain for the optimized project, where it is possible to see a considerable reduction in the gain from the walls due to the increase of insulation thickness defined by the optimizer.

4.5.2 Parametric study

The parametric study was carried out by setting the parameters at the optimized values and varying only one for each analysis. The results presented in Figures 16 to 17 show the expected energy consumption and the payback as a function of the insulation thickness and number of panels.

Finally, the weighted sum objective J is shown in Figures 18a to 18c varying all the parameters. In each result, the line representing the optimized parameter value is also displayed.

Starting from Figure 18, it is possible to observe that the optimum value found is in the region that would be expected, being an intermediate value within the range for insulation and number of panels and the minimum value for ventilation. Analyzing each objective separately, Figure 16 shows how the increase in insulation thickness and the number of panels tend to reduce the demand for cooling. The former, due to the reduction in heat exchange with the external environment. The latter, due to the shading effect that the solar panels generate on the roof. Figure 17 shows how the effect of the cost of installation and maintenance of the construction components affects the payback-time, in which for the two parameters presented the optimal value is located somewhere in the intermediate range of the parameters. In all cases, the optimizer had to make a trade-off in search of the optimum value that best brings the weight balance defined for the case study, from 50% for E_ac and 50% for τ.

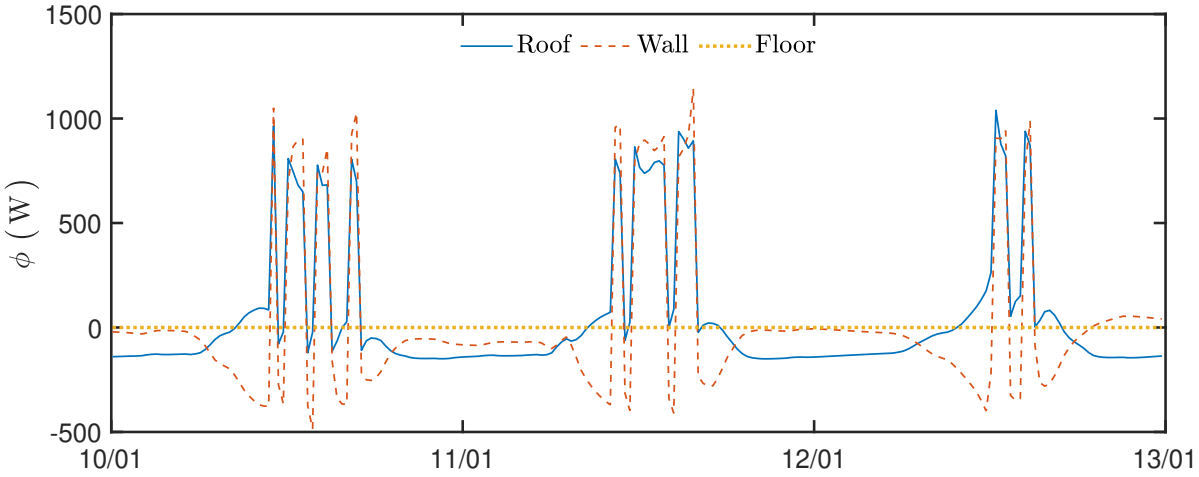

(a)

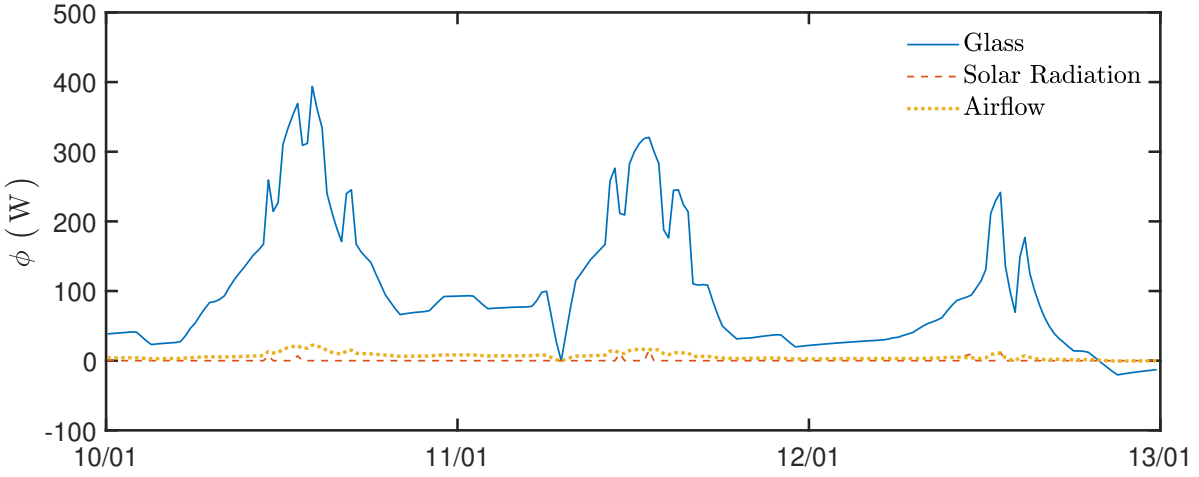

(b)

Figure 15. *Optimized project wall thermal gains (a) and other thermal gains (b).*

4.6 Multi-objective optimization

The study using the multi-objective optimization comprises a total of generations of $N_g = 50$ and a population size of $N_u = 16$ individuals, which represents 800 runs. No convergence-based stopping criterion is defined for this multi-objective optimization. The criteria adopted are the total number of generations and the self intervention to conclude the optimization when the result seems appropriate.

The optimization results are presented in the form of the Pareto-front related to the values of J_1 and J_2. In Figure 19a, the Pareto-front is presented in its final position, not only after 50 generations but also for previous ones (5 and 15). Including these predecessor generations, it is possible to verify that with 15 generations, the location of the front is considerably close to the final one, hence, 15 generations seems to be enough to optimize the case study. With 5 generations, the individual's location is close to the place of the final Pareto-front, which can be a possible optimization although the coarse generation process. The result of multi-objective optimization after 50 generations is denoted as *best-known Pareto-front*.

Figure 19b aims to compare the result of mono-objective optimization with the Pareto-front obtained from multi-objective optimization. Generation 4 is chosen for comparison because it has a number of simulations (64 runs) similar to the total performed in the mono-objective (62

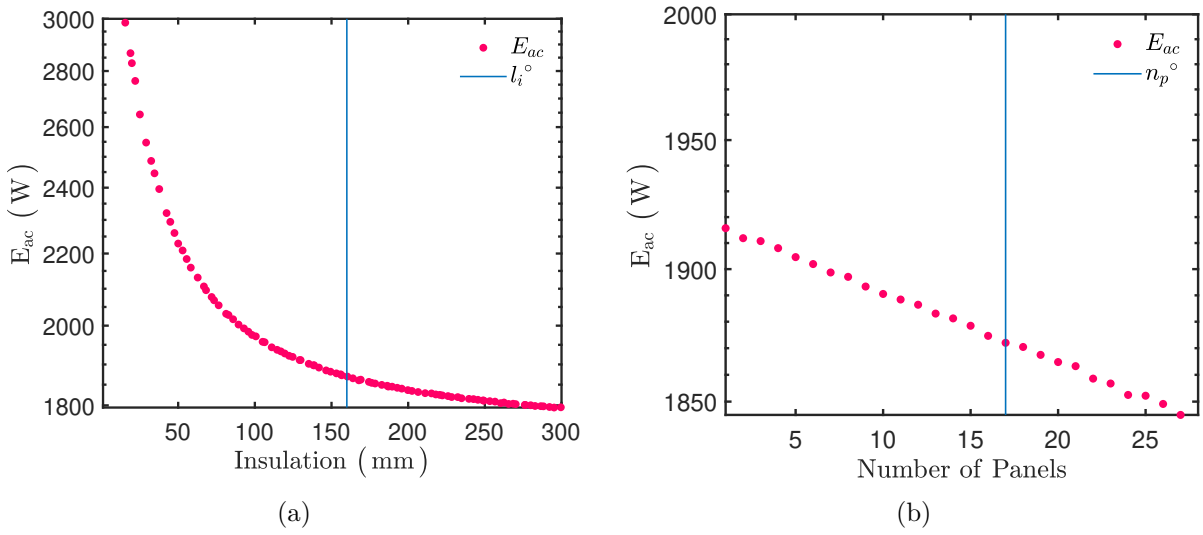

Figure 16. *Parametric analysis of the energy consumption varying the insulation thickness (a) and the number of panels (b).*

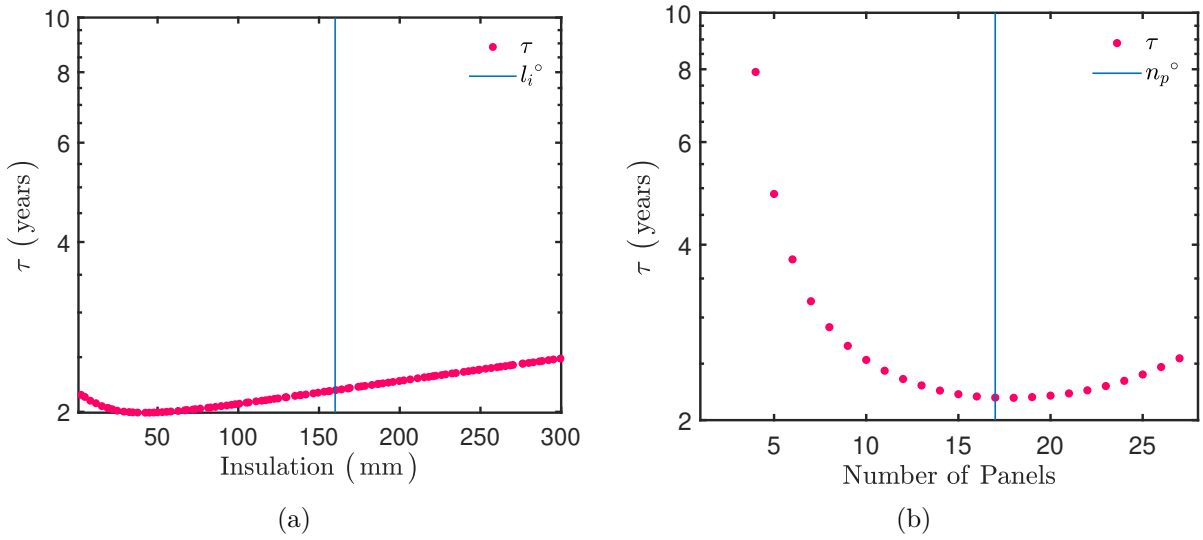

Figure 17. *Parametric analysis of the construction cost modifying the insulation thickness (a) and the number of panels (b).*

runs), thus having a comparable computer run time needed to reach the results. From this result, it is possible to observe that despite the mono-optimization being close to the Pareto-front (considering the entire objective space), the multi-objective optimization shows better performance with the same computational effort.

Figure 20a presents the annual cooling demand, while Figure 20b the payback-time, for three different elements of the Pareto-front, One element is associated to a lower value for cooling demand (Bias in E_{ac}). A second one is linked to a lower value for the payback-time (Bias in τ), and the last element is the one with an average result, among the objectives. Figure 20c shows the three selected elements of the Pareto-front and Table 5, the respective parameters and objective values.

The results presented in Figures 20a and 20b demonstrate the considerable variation between elements of the Pareto-front within each objective. It is also interesting to note how the mono-objective optimization had a result very similar to the Mean multi-objective element in the cooling demand but presented the highest result among all in the optimization of τ. Such

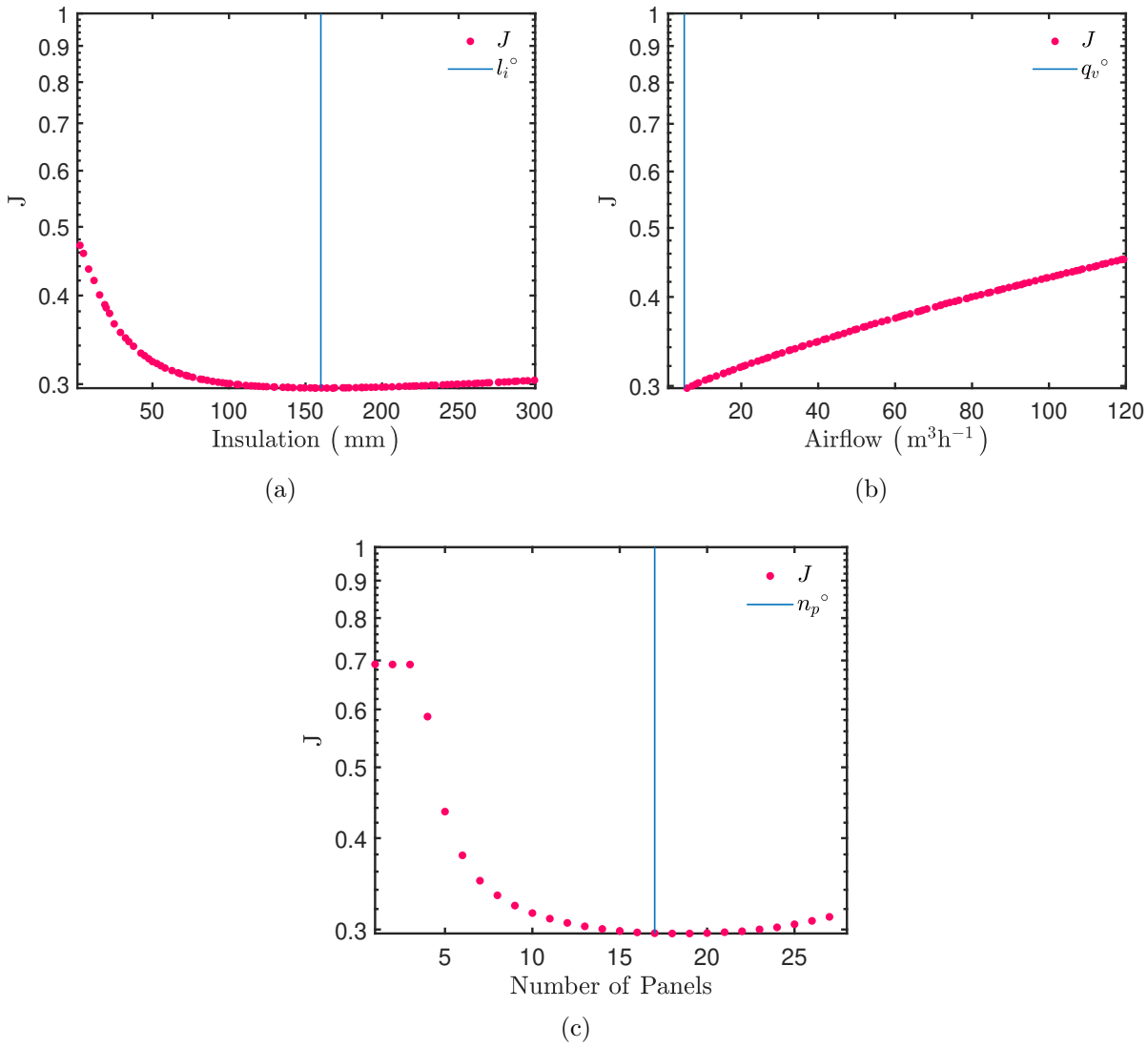

Figure 18. *The optimized objective concerning the variation of insulation thickness (a), ventilation airflow (b) and the number of panels (c).*

behaviour demonstrates that a better balance of the weights defined in the weighted approach may be necessary.

Table 6 presents the computer CPU run time required to compute the solution for the mono- and multi-objective optimization, using an `Intel Core i5-8265U` 1.6 GHz CPU and 8 GB RAM. The computational ratio scales with 4 between mono and multi-objective (with 15 generations) using a standard laptop computer. Indeed the number of simulations is higher for the second case. Thus, for building engineers or architects, the mono-objective optimization approach may be an interesting compromise for real case applications. The multi-objective optimization with 50 generations has a very important computational cost compared to the small gains in the pareto front.

5 Conclusion

In the context of near-zero energy buildings, solar power and low-cost construction, it is of great importance to provide effective optimization algorithms to be combined to building energy simulation tools. Hence, this paper presented optimization models integrated to a BES tool to

(a) (b)

Figure 19. *Pareto-front for different generations in the optimization process (a). Comparing with the optimized project of the mono-objective optimization (b).*

Table 5. *Parameters and objectives for Pareto-front bias analyses.*

Project	$l_i \left[\mathsf{mm}\right]$	$q_v \left[\mathsf{m3/h}\right]$	$n_p \left[-\right]$	$E_{ac} \left[\mathsf{kWh}\right]$	$\tau \left[\mathsf{years}\right]$
Bias in E_{ac}	299.6	5.0	26	1779	2.7
Mean	144.0	5.0	17	1888	2.15
Bias in N_p	43.3	5.0	17	2307	1.99

Table 6. *Run time, comparing mono- and multi-objective approaches.*

Optimization	Number of simulations	Run time $\left[\mathsf{h}\right]$
Mono	62	3.39
Multi- Gen 15	240	11.8
Multi- Gen 50	800	35.7

simplify the optimization procedure. At the same time, when using a communication interface with external models together with optimization algorithms developed in Python scripts, it is possible to improve the tool versatility so that models can be updated or replace without requiring any assistance from the development team, which is of paramount importance as new products can be rapidly available to a growing nZEB market.

Using a case study based on BESTEST 910, adapted to local conditions for a hot Brazilian climate, the objective of the study is to optimize the cooling demand and the investment payback-time by increasing solar energy generation and reducing the costs associated to the building envelope and to the PV panels associated. The solar panels optimization is one of the highlights of this study because it takes advantage of the high solar radiation in the chosen city as well as the potential of the pixel-counting technique implemented in `Domus`, in terms of accuracy and rapidness.

Two optimization approaches were tested using free-available libraries. A mono-objective model that aims to be more specific with a single optimized result, even when operating with more than one objective. And a multi-objective model, bringing more detailed results and pro-

(a)

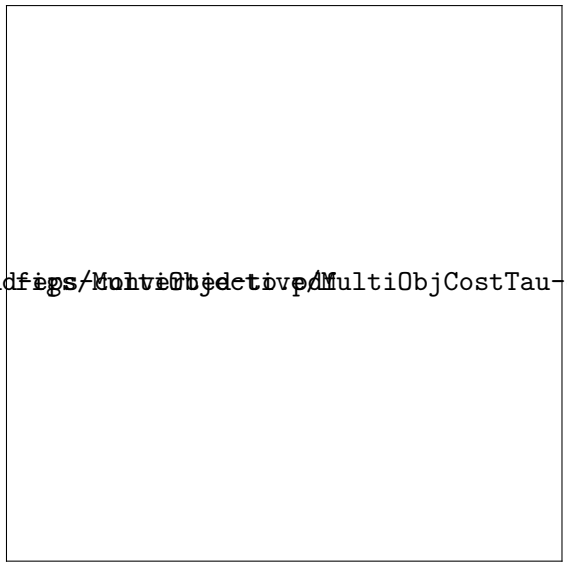

(b)

(c)

Figure 20. *Annual cooling demand (a) and τ value (b) for three values of the Pareto-front, one tending to E_{ac}, another to τ and finally a mean value without tending to any of the objectives (c).*

viding more freedom to wisely select the optimization objectives. It is possible to conclude that the multi-objective optimization presents better results, although with a higher computational burden until reaching a result close to the *best-known Pareto-front* (around 15 generations and 11h of run time). The single-objective optimization can satisfy the purpose of optimizing the desired parameters, reaching the stopping criteria after less than 4 hours of simulation. However, as it is possible to observe in Section 4.6, it does not find the closest value to the global-optimum region.

Further work is intended to include window type in the optimization process and promote the use of different mono-objective optimization algorithms to increase reliability. In addition, more sophisticated stopping criteria for multi-objective optimization can bring an important evolution for the methodology. Furthermore, the pixel counting can be more explored for evaluation of

solar radiation availability in complex scenarios such as real district analysis.

Acknowledgments

The authors acknowledge the Carnot Institute "Energies du Futur" through the project MN4BAT, as well as the French and Brazilian agencies for their financial support through the project CAPES-COFECUB, and the eco-SESA Cross-Disciplinary Program (ANR-15-IDEX-02). The authors also acknowledge the French and Brazilian agencies for their financial supports through the project CAPES–COFECUB, as well as the CNPQ of the Brazilian Ministry of Education and of the Ministry of Science, Technology and Innovation, respectively, for co-funding.

References

[1] EPE Empresa de Pesquisa Energética. Brazilian energy balance 2019. *Rio de Janeiro: EPE*, 2019. 1

[2] Air Infiltration, Ventilation Centre, P.G. Schild, and M. Mysen. *Energy Technology Perspectives 2017: Catalyzing Energy Technology Transformations*. International Energy Agency, Paris, 2017. 1

[3] Joeri Rogelj, Drew Shindell, Kejun Jiang, Solomone Fifita, Piers Forster, Veronika Ginzburg, Collins Handa, Haroon Kheshgi, Shigeki Kobayashi, Elmar Kriegler, et al. Mitigation pathways compatible with 1.5 c in the context of sustainable development. Technical report, Intergovernmental Panel on Climate Change, 2018. 1

[4] IEA. *SHC Task 40/ECBCS Annex 52, Towards Net Zero Energy Solar Buildings*. International Energy Agency, Canada, 2008. 1

[5] European Parliament. Directive 2010/31/eu of the european parliament and of council of 19 may 2010 on the energy performance of buildings. *Official journal of the European Union*, page 1325, 2010. 1

[6] Ayman Mohamed, Ala Hasan, and Kai Sirén. Fulfillment of net-zero energy building (nzeb) with four metrics in a single family house with different heating alternatives. *Applied Energy*, 114:385 – 399, 2014. 1

[7] Silvia Guillén-Lambea, Beatriz Rodríguez-Soria, and José M. Marín. Comfort settings and energy demand for residential nzeb in warm climates. *Applied Energy*, 202:471 – 486, 2017. 1

[8] Fabrizio Ascione, Rosa Francesca De Masi, Filippo de Rossi, Silvia Ruggiero, and Giuseppe Peter Vanoli. Optimization of building envelope design for nzebs in mediterranean climate: Performance analysis of residential case study. *Applied Energy*, 183:938 – 957, 2016. 1

[9] S. El Sayary and O. Omar. Designing a bim energy-consumption template to calculate and achieve a net-zero-energy house. *Solar Energy*, 216:315–320, 2021. 1

[10] S. Beazley, E. Heffernan, and T. J. McCarthy. Enhancing energy efficiency in residential buildings through the use of bim: The case for embedding parameters during design. *Energy Procedia*, 121:57–64, 2017. Improving Residential Energy Efficiency International Conference, IREE 2017. 1

[11] Ralph Evins. A review of computational optimisation methods applied to sustainable building design. *Renewable and sustainable energy reviews*, 22:230–245, 2013. 2

[12] I. Costa-Carrapiço, R. Raslan, and J. N. González. A systematic review of genetic algorithm-based multi-objective optimisation for building retrofitting strategies towards energy efficiency. *Energy and Buildings*, 210:109690, 2020. 2

[13] O. Pasichnyi, F. Levihn, H. Shahrokni, J. Wallin, and O. Kordas. Data-driven strategic planning of building energy retrofitting: The case of stockholm. *Journal of Cleaner Production*, 233:546–560, 2019. 2

[14] M. Heidarinejad, N. Mattise, M. Dahlhausen, K. Sharma, K. Benne, D. Macumber, L. Brackney, and J. Srebric. Demonstration of reduced-order urban scale building energy models. *Energy and Buildings*, 156:17–28, 2017. 2

[15] V. Milic, K. Ekelow, M. Andersson, and B. Moshfegh. Evaluation of energy renovation strategies for 12 historic building types using lcc optimization. *Energy and Buildings*, 197:156–170, 2019. 2

[16] G. Guariso and M. Sangiorgio. Multi-objective planning of building stock renovation. *Energy Policy*, 130:101–110, 2019. 2, 4

[17] M-L. Pannier, T. Recht, M. Robillart, P. Schalbart, B. Peuportier, and L. Mora. Identifying optimal renovation schedules for building portfolios: Application in a social housing context under multi-year funding constraints. *Energy and Buildings*, 250:111290, 2021. 2

[18] Abdullah Konak, David W Coit, and Alice E Smith. Multi-objective optimization using genetic algorithms: A tutorial. *Reliability Engineering & System Safety*, 91(9):992–1007, 2006. 2, 6

[19] Kalyanmoy Deb, Amrit Pratap, Sameer Agarwal, and TAMT Meyarivan. A fast and elitist multiobjective genetic algorithm: Nsga-ii. *IEEE transactions on evolutionary computation*, 6(2):182–197, 2002. 2

[20] Kalyanmoy Deb and Himanshu Jain. An evolutionary many-objective optimization algorithm using reference-point-based nondominated sorting approach, part i: solving problems with box constraints. *IEEE transactions on evolutionary computation*, 18(4):577–601, 2013. 2

[21] G Fraisse, B Souyri, F Wurtz, X Brunotte, P Enciu, Bruno Peuportier, M Robillart, N Stathopoulos, S Truchet, E Francois, et al. Towards holistic building optimization using a computing environment that enable interoperability between numerical tools. In *International Conference on Efficiency, Cost, Optimization, Simulation and Environmental Impact of Energy Systems*, 2018. 2

[22] N. Mendes, R. C. L. F. Oliveira, and G. H. dos Santos. Domus 2.0: a whole-building hygrothermal simulation program. In *Proceedings of the 8th International Building Performance Simulation Association Conference*, pages 863–870, Eindhoven, Netherlands, August 2003. 2

[23] N. Mendes, R. M. Barbosa, R. Z. Freire, and R. C. L. F. Oliveira. A simulation environment for performance analysis of HVAC systems. *Building Simulation*, 1(2):129–143, 2008. 2

[24] R. M. Barbosa and N. Mendes. Combined simulation of central HVAC systems with a whole-building hygrothermal model. *Energy and Buildings*, 40(3):276–288, 2008. 2

[25] R. Z. Freire, M. O. Abadie, and N. Mendes. Integration of natural ventilation models in the hygrothermal and energy simulation program PowerDomus. In *Proceedings of the 11th International Building Performance Simulation Association Conference*, pages 1037–1044, Glasgow, Scotland, July 2009. 2

[26] R. Z. Freire, W. Mazuroski, M. O. Abadie, and N. Mendes. Capacitive effect on the heat transfer through building glazing systems. *Applied Energy*, 88(12):4310–4319, 2011. 2, 11

[27] R. Z. Freire, M. Abadie, and N. Mendes. Numerical simulation of building-integrated photovoltaic systems. In *Proceedings of the 13th Brazilian Congress of Thermal Sciences and Engineering (ENCIT 2010)*, Uberlândia, MG, Brazil, December 2010. 3, 4, 14

[28] Ana Paula de Almeida Rocha, Gilberto Reynoso-Meza, Ricardo CLF Oliveira, and Nathan Mendes. A pixel counting based method for designing shading devices in buildings considering energy efficiency, daylight use and fading protection. *Applied Energy*, 262:114497, 2020. 3, 11

[29] Ana Paula de Almeida Rocha, Ricardo CLF Oliveira, and Nathan Mendes. Experimental validation and comparison of direct solar shading calculations within building energy simulation tools: Polygon clipping and pixel counting techniques. *Solar Energy*, 158:462–473, 2017. 3

[30] Ana Paula de Almeida Rocha, Auline Rodler, Ricardo CLF Oliveira, Joseph Virgone, and Nathan Mendes. A pixel counting technique for sun patch assessment within building enclosures. *Solar Energy*, 184:173–186, 2019. 3, 11

[31] Shan K. Wang. *Handbook of Air Conditioning and Refrigeration*. McGraw-Hill Education, 2nd edition, 2000. 3

[32] Julien Berger and Nathan Mendes. An innovative method for the design of high energy performance building envelopes. *Applied Energy*, 190(Supplement C):266 – 277, 2017. 3

[33] Air Infiltration, Ventilation Centre, P.G. Schild, and M. Mysen. *Technical Note AIVC 65: Recommendations on Specific Fan Power and Fan System Efficiency*. International Energy Agency, Belgium, 2009. 4

[34] C. G. Lewin. An early book on compound interest. *Journal of the Institute of Actuaries*, 96:121–132, 1970. 4

[35] M. Peters, T. S. Schmidt, D. Wiederkehr, and M. Schneider. Shedding light on solar technologies—a techno-economic assessment and its policy implications. *Energy Policy*, 39(10):6422–6439, 2011. Sustainability of biofuels. 4

[36] A. Franco. Methods for the sustainable design of solar energy systems for industrial process heat. *Sustainability*, 12(12), 2020. 4

[37] W.D. Short. Method for including operation and maintenance costs in the economic analysis of active solar energy systems. Technical report, U.S. Department of Energy, Office of Scientific and Technical Information, 1986. 4

[38] FMI-Standard. FMI-Standard Functional Mock-up Interface. `fmi-standard.org`, 2017. Accessed: 2017-07-03. 4

[39] Eric Brochu, Vlad M. Cora, and Nando de Freitas. A tutorial on bayesian optimization of expensive cost functions, with application to active user modeling and hierarchical reinforcement learning. *ArXiv*, abs/1012.2599, 2010. 5

[40] Jonas Mockus. Application of bayesian approach to numerical methods of global and stochastic optimization. *Journal of Global Optimization*, 4(4):347–365, 1994.

[41] Y. Wang, A.W. Kandeal, A. Swidan, S. W. Sharshir, G. B. Abdelaziz, M.A. Halim, A.E. Kabeel, and N. Yang. Prediction of tubular solar still performance by machine learning integrated with bayesian optimization algorithm. *Applied Thermal Engineering*, 184:116233, 2021. 5

[42] F. Pedregosa, G. Varoquaux, A. Gramfort, V. Michel, B. Thirion, O. Grisel, M. Blondel, P. Prettenhofer, R. Weiss, V. Dubourg, J. Vanderplas, A. Passos, D. Cournapeau, M. Brucher, M. Perrot, and E. Duchesnay. Scikit-learn: Machine learning in Python. *Journal of Machine Learning Research*, 12:2825–2830, 2011. 6

[43] Himanshu Jain and Kalyanmoy Deb. An evolutionary many-objective optimization algorithm using reference-point based nondominated sorting approach, part ii: handling constraints and extending to an adaptive approach. *IEEE Transactions on evolutionary computation*, 18(4):602–622, 2013. 6, 8

[44] Félix-Antoine Fortin, François-Michel De Rainville, Marc-André Gardner, Marc Parizeau, and Christian Gagné. DEAP: Evolutionary algorithms made easy. *Journal of Machine Learning Research*, 13:2171–2175, jul 2012. 8

[45] Marcin Molga and Czesław Smutnicki. Test functions for optimization needs. *Test functions for optimization needs*, 101, 2005. 9

[46] Zhengbing Hu. *Advances in Computer Science for Engineering and Education II*, volume 938. Springer, 2019. 9

[47] Brazilian Electricity Regulatory Agency (ANEEL). General information database: BIG. http://www.aneel.gov.br/ranking-das-tarifas, 2020. [Online; accessed 04/10/2020]. 10

[48] Brazil. Chamber of Electric Energy Commercialization (CCEE). https://www.ccee.org.br/, 2020. [Online; accessed 04/10/2020].

[49] Solar Panels Information and Brazil. Marketplace. https://www.portalsolar.com.br/, 2020. [Online; accessed 04/10/2020]. 10

[50] R.Z. Freire, Marc O. Abadie, Walter Mazuroski, and N. Mendes. Analysis of Two Different Approaches to Solve the Heat Transfer Through Single- and Double-Glazing Systems in Whole Building Energy Simulation. In *COBEM 2009*, pages 1–6, Brazil, 2009. 11

[51] S.R. Castillo, L.M. Moura, and N. Mendes. An algorithm to determine radiative properties of glazing systems using simple window performance indicators. In *COBEM 2017*, pages 1–6, Brazil, 2017.

[52] S.R. Castillo, N. Mendes, and L.M. Moura. Validation and Application of a Numerical Code for Energy Performance of Glazing Systems based on Semi-Transparent Organic Photovoltaic Elements. In *Building Simulation Conference (BS 2019)*, pages 1–8, Italy, 2019. 11

[53] Ana Paula de Almeida Rocha, Nathan Mendes, and Ricardo CLF Oliveira. Domus method for predicting sunlit areas on interior surfaces. *Ambiente Construído [online]*, 184:83–95, 2018. 11

Construction parameters of the case study

Table 7. *Wall Construction (NSI/ASHRAE Standard 140-2007).*

Element	k [W/mK]	e [m]	U [W/m^{2}K]	R [m^{2}K/W]	ρ [kg/m^3]	cp [J/kgK]
Int. Surface Coef.	—	—	8.290	0.121	—	—
Concrete Block	0.510	0.100	5.100	0.196	400	1000
Foam Insulation	0.040	0.0615	0.651	1.537	10	1400
Wood Siding	0.140	0.009	15.556	0.064	530	900
Ext. Surface Coef.	—	—	29.300	0.034	—	—
Overall, air-to-air	—	—	0.512	1.952	—	—

Table 8. *Roof Construction (NSI/ASHRAE Standard 140-2007).*

Element	k [W/mK]	e [m]	U [W/m^{2}K]	R [m^{2}K/W]	ρ [kg/m^3]	cp [J/kgK]
Int. Surface Coef.	—	—	8.290	0.121	—	—
Concrete Block	0.160	0.010	16.00	0.063	950	840
Foam Insulation	0.040	0.1118	0.358	2.794	11	840
Wood Siding	0.140	0.019	7.368	0.136	530	900
Ext. Surface Coef.	—	—	29.300	0.034	—	—
Overall, air-to-air	—	—	0.514	1.944	—	—

Table 9. *Window properties (NSI/ASHRAE Standard 140-2007).*

Element	Properties
Extinction coeficiente	0.0196 $\left[\mathsf{mm}\right]$
Number of panes	2
Pane thickness	3.175 $\left[\mathsf{mm}\right]$
Air-gap thickness	13 $\left[\mathsf{mm}\right]$
Index of refraction	1.526
Normal direct-beam transmittance through one pane	0.86156
Thermal Conductivity of glass	1.06 $\left[\mathsf{W/mK}\right]$
Conductance of each glass pane	333 $\left[\mathsf{W/m^2.K}\right]$
Combined radiative and convective coefficient of air gap	6.297 $\left[\mathsf{W/m^2K}\right]$
Exterior combined surface coefficient	21.00 $\left[\mathsf{W/m^2K}\right]$
Interior combined surface coefficient	8.29 $\left[\mathsf{W/m^2K}\right]$
U-value from interior air to ambient air	3.0 $\left[\mathsf{W/m^2K}\right]$
Hemispherical infrared emittance of ordinary uncoated glass	0.9
Density of glass	2500 $\left[\mathsf{kg/m^3}\right]$
Specific heat of glass	750 $\left[\mathsf{J/kgK}\right]$
Interior shade devices	None
Double-pane shading coefficient at normal incidence	0.907
Double-pane solar heat gain coefficient at normal incidence	0.789